HYBRID LINEAR / BILINEAR TIME-SCALE ANALYSIS

Martin Pasquier

Ecole Nationale Supérieure de Télécommunications
46, rue Barrault, 75634 Paris Cedex 13, France
pasquier@email.enst.fr

Paulo Gonçalvès and Richard Baraniuk*

Department of Electrical and Computer Engineering
Rice University, Houston, Texas 77005, USA
gpaulo@ece.rice.edu, richb@rice.edu
Fax: (713) 524-5237
http://www-dsp.rice.edu
Corresponding author: R. Baraniuk

Submitted to *IEEE Transactions on Signal Processing*, July 1996
EDICS Number SP–2.3.1 Time-Frequency Signal Analysis

Abstract

We introduce a new method for the time-scale analysis of non-stationary signals. Our work leverages the success of the "time-frequency distribution series / cross-term deleted representations" into the time-scale domain to match wide-band signals that are better modeled in terms of time shifts and scale changes than in terms of time and frequency shifts. Using a wavelet decomposition and the Bertrand time-scale distribution, we locally balance linearity and bilinearity in order to provide good resolution while suppressing troublesome interference components. The theory of frames provides a unifying perspective for cross-term deleted representations in general.

*This work was supported by the National Science Foundation, grant no. MIP–9457438, and the Office of Naval Research, grant no. N00014–95–1–0849.

1 Introduction

By displaying the time-varying frequency content of a non-stationary signal in terms of time and frequency variables, joint time-frequency and time-scale representations can reveal subtle features that remain hidden from other methods of analysis. Each type of representation matches a different class of signals. Time-frequency representations are covariant to time and frequency shifts and match signals with constant-bandwidth structure, such as narrow-band radar signals. Time-scale representations are covariant to time shifts and scale changes and match signals with proportional-bandwidth structure, such as wide-band sonar and acoustic signals. Many different representations exist, both linear and nonlinear.

Linear representations such as the short-time Fourier and Gabor time-frequency representations and the wavelet time-scale representation offer the benefit of simple interpretation at the expense of poor resolution. Bilinear representations such as the Wigner time-frequency distribution and the Bertrand time-scale distribution were developed as high resolution alternatives. While the nonlinearity of the bilinear distributions sharpens the representation of local signal structure, it simultaneously generates interference between widely separated components that degrades the representation of global structure. Traditionally, nonlinear interference due to these cross-components has been suppressed via smoothing over the time-frequency and time-scale planes [1, 2].

In [3, 4], Qian, Morris, and Chen introduced an alternative approach to time-frequency analysis that features an explicit and controllable linear vs. bilinear tradeoff. First the signal is represented in terms of a discrete sum of time-frequency concentrated atoms via a linear Gabor transform. Then the Wigner distribution, evaluated on this linear signal decomposition rather than on the signal itself, separates into two distinct components: the Wigner auto-components of the atoms (the quasi-linear part of the representation) and the Wigner cross-components of the atoms (the bilinear part of the representation). By limiting the number of cross-components entering into the sum, we can locally control the degree of nonlinearity of the time-frequency representation and furthermore tune it for maximum concentration with minimum cross-components.

This time-frequency decomposition performs very well, but it is matched only to signals possessing a constant-bandwidth structure. In this paper, we extend the concept of hybrid linear/bilinear analysis to the time-scale plane. Our approach is based on the linear wavelet transform and the bilinear Bertrand distribution. In the process of our development, we gain new insights into the procedure of Qian, Morris, and Chen. In Section 2, we briefly review their approach to quasi-linearizing the Wigner distribution. In Section 3, we transpose the problem of hybrid linear/bilinear analysis to time-scale and propose a frame-based solution. After discussing an implementation of this new method in Section 4, we close with conclusions.

2 Hybrid Time-Frequency Analysis

A hybrid linear/bilinear system for time-frequency analysis consists of three components:

1. a bilinear time-frequency mapping,
2. a discrete linear signal decomposition based on time-frequency concentrated "atoms,"
3. a rule for determining which cross-components to include in the overall signal representation.

In [3, 4], Qian, Morris, and Chen utilize the bilinear Wigner distribution, a linear Gabor transform with a Gaussian window, and a Manhattan distance criterion.

2.1 Wigner distribution

The Wigner distribution is in many senses the central bilinear time-frequency distribution [1]. The cross-Wigner distribution of two signals r and s is defined as[1]

$$W_{r,s}(t,f) \;=\; \int r^*\left(t-\frac{\tau}{2}\right) s\left(t+\frac{\tau}{2}\right) e^{-j2\pi f\tau}\, d\tau. \tag{1}$$

When $s=r$, we have the Wigner distribution $W_s(t,f)$.

The excellent time-frequency localization properties of the *auto-components* of the Wigner distribution result from its bilinear, "matched filter" structure. This bilinearity also results in *cross-components*, which, unfortunately, impair its representation of multi-component signals. The Wigner distribution of the multi-component signal $s(t)=\sum_{i=1}^N s_i(t)$ reads as

$$W_s(t,f) \;=\; \sum_{i=1}^N W_{s_i}(t,f) \;+\; \sum_{i\neq j} W_{s_i,s_j}(t,f). \tag{2}$$

The first sum comprises the auto-components, the second the cross-components. Traditionally, Wigner distribution cross-components have been suppressed via smoothing over the time-frequency plane. Two-dimensional convolution yields a distribution in Cohen's class of time-frequency representations [1]; affine convolution yields a distribution in the affine class of time-scale representations [2].

In [3, 4], Qian, Morris, and Chen introduced an alternative approach to cross-component suppression that marries the decomposition (2) with the linear Gabor transform.

2.2 Gabor transform

The Gabor transform represents a signal s in terms of time-frequency atoms [5]:

$$s(t) \;=\; \sum_{(m,n)} c_{m,n}\,\phi_{m,n}(t), \quad (m,n)\in\mathbb{Z}^2, \tag{3}$$

$$c_{m,n} \;=\; \left\langle s,\, \widetilde{\phi}_{m,n}\right\rangle \;=\; \int s(t)\left(\widetilde{\phi}_{m,n}(t)\right)^* dt. \tag{4}$$

[1]Throughout this paper, integration bounds run from $-\infty$ to $+\infty$.

The synthesis atoms

$$\phi_{m,n}(t) \;=\; g(t - nt_0)\, e^{j2\pi m f_0 t}, \quad t_0 f_0 \leq 1,$$

are obtained by shifting one basic atom g to various times nt_0 and frequencies mf_0 in the time-frequency plane. The analysis atoms $\widetilde{\phi}_{m,n}$, which are different from the synthesis atoms in general, comprise the *dual basis*. The product $t_0 f_0$ corresponds to the density of placement of the atoms in the time-frequency plane.

The Gaussian function is the natural choice for the basic atom g. Since it is the most concentrated signal in time-frequency, its associated Gabor representation is as local as possible. Furthermore, the Wigner distribution of a Gaussian function is strictly positive and so has a correct energetic interpretation. The key drawback to Gaussian synthesis atoms is that for time-frequency sampling densities $t_0 f_0$ close to unity, the corresponding dual basis functions have extremely poor localization properties (Balian-Low theorem [5, p. 108]) plus a spiky structure that does not allow a numerically stable reconstruction. Qian and Chen deal with this problem by introducing redundancy ($t_0 f_0 \ll 1$) in the Gabor transform until both the basis and dual basis atoms resemble shifted, modulated Gaussians [4]. They term such a representation an "orthogonal-like" Gabor decomposition.

2.3 Hybrid System

Using Gaussian time-frequency atoms as building blocks, Qian, Morris, and Chen substitute (3) into (1) to decompose the Wigner distribution into a *time-frequency distribution series* — a sum of auto- and cross-Wigner distributions [3, 4]

$$W_s(t,f) \;=\; \sum_{(m,n)} |c_{m,n}|^2\, W_{\phi_{m,n}}(t,f) \;+ \sum_{(m,n)\neq(m',n')} c_{m,n}\, c^*_{m',n'}\, W_{\phi_{m,n},\,\phi_{m',n'}}(t,f) \tag{5}$$

The first sum corresponds to the "quasi-linear part" of the representation; it is manifestly positive and indicates the gross features of the signal. The second sum corresponds to the "bilinear part" of the representation; it takes on both positive and negative values. Locally it serves to concentrate the features of the signal in the representation, while globally it creates interference components between nonadjacent portions of the signal.

By limiting the range of the second sum to include only (m,n) close to (m',n'), we can retain the useful, local nonlinear interactions but suppress the noxious, global interactions. Given the circular or elliptical symmetry of the Gaussian atoms of the Gabor decomposition, a Euclidean distance metric seems natural to measure closeness. For computational simplicity, Qian and Chen approximate this measure with an l_∞ metric (the so-called "Manhattan distance") $D_{\mathrm{M}}[(m,n),(m',n')] = |m-m'| \;+\; |n-n'|$. The hybrid linear/bilinear time-frequency representation of Qian, Morris, and Chen then corresponds to

$$\widetilde{W}_s(t,f) \;=\; \sum_{(m,n)} |c_{m,n}|^2\, W_{\phi_{m,n}}(t,f) \;+ \sum_{0<D_{\mathrm{M}}[(m,n),(m',n')]\leq\delta} c_{m,n}\, c^*_{m',n'}\, W_{\phi_{m,n},\,\phi_{m',n'}}(t,f). \tag{6}$$

The threshold distance δ controls the localization *vs.* interference tradeoff.

3 Hybrid Time-Scale Analysis

The hybrid linear/bilinear time-frequency representation of Qian, Morris, and Chen performs very well, but it matches only signals with a constant-bandwidth structure. For signals exhibiting a proportional bandwidth, wide-band structure, a time-scale analysis is more appropriate. To transfer the linear/bilinear decomposition concept from the time-frequency plane to the time-scale plane, we must find wide-band substitutes for the Wigner distribution, Gabor transform, Gaussian atom, and Euclidean distance.

3.1 Bertrand Distribution

The unitary Bertrand distribution can be considered as a central bilinear time-scale distribution [6]. The cross-Bertrand distribution of two signals r and s is defined in terms of their Fourier transforms R and S as

$$B_{r,s}(t,f) \;=\; f \int R(\lambda(u)f)\, S^*(\lambda(-u)f)\, e^{j2\pi t f u}\, \mu(u)\, du, \tag{7}$$

with $\lambda(u) = \frac{u}{1-e^{-u}}$ and $\mu(u) = \sqrt{\lambda(u)\lambda(-u)}$. When $S = R$, we have the Bertrand distribution $B_s(t,f)$. Like the Wigner distribution, the Bertrand distribution inherits both its good localization and problematic cross-components [7] from its bilinear structure.

3.2 Wavelet Transform

The wavelet transform plays a role analogous to the Gabor transform in time-scale analysis. The wavelet transform also represents signals in terms of time-frequency atoms [5]:

$$s(t) \;=\; \sum_{(m,n)} d_{m,n}\, \psi_{m,n}(t), \quad (m,n) \in \mathbb{Z}^2, \tag{8}$$

$$d_{m,n} \;=\; \left\langle s, \widetilde{\psi}_{m,n} \right\rangle. \tag{9}$$

Given a bandpass mother wavelet function h centered at frequency f_c, we create the synthesis atoms

$$\psi_{m,n}(t) \;=\; a_0^{-m/2}\, h(a_0^{-m} t - n t_0),$$

by shifting and scaling h to various times $n t_0 a_0^m$ and frequencies $a_0^{-m} f_c$ in the time-frequency plane. The proportional-bandwidth analysis of the wavelet transform matches wide-band signals.

For the mother wavelet, we choose the Klauder function [5, p. 41], [8]

$$H(f) \;=\; f^{\beta}\, e^{-\alpha f}, \qquad \alpha > 0,\ \beta > 0,\ f > 0, \tag{10}$$

expressed here in the frequency domain. The parameter β controls the Q factor of the wavelet, while α controls its extent (see Figure 1). The properties of this function in time-scale mirror those of the Gaussian in time-frequency. First, the Klauder function is the most concentrated signal in time-scale [8], meaning that the associated wavelet representation is as local as possible. Second, the Bertrand distribution of a Klauder wavelet is positive [9], giving it a correct energetic interpretation. The key drawback to Klauder synthesis atoms is that for low time-scale sampling densities the corresponding dual basis functions have poor localization properties. To better understand the links between bases and dual bases using the Klauder wavelet, we turn now to the theory of frames.

3.3 Frames

A *frame* is a family of functions $\{\gamma_{m,n}\}$ in a Hilbert space with the property that there exist two *frame bounds* $0 < A \leq B < \infty$ such that for all signals s in the space [5]

$$A\,\|s\|^2 \;\leq\; \sum_{(m,n)} |\langle s, \gamma_{m,n}\rangle|^2 \;\leq\; B\,\|s\|^2$$

The frame bounds can be estimated numerically given the frame. Depending on their values, we can distinguish several different categories of frames:

1. When $A = B$, we have a *tight frame* and the signal representation

$$s(t) \;=\; A^{-1} \sum_{(m,n)} \langle s, \gamma_{m,n}\rangle\, \gamma_{m,n}(t). \tag{11}$$

   The value A measures the degree of redundancy of a tight frame. In particular, when $A = B = 1$, the family $\{\gamma_{m,n}\}$ corresponds to an orthonormal basis.

2. When $A \approx B$, we have a *snug frame*. In this case, the signal representation (11) holds to a close approximation.

3. When $A \neq B$, the signal representation (11) does not hold. In this case, we must construct a different *dual frame* for analysis.

The theory of frames furnishes an elegant characterization of the Gabor and wavelet transforms. In particular, the concept of a snug frame provides insight into the "orthogonal-like" Gabor decomposition introduced in Section 2.2 [4]. Numerical computation of the frame bounds for g Gaussian ($g(t) = e^{-t^2/2}$) and $t_0 f_0 = 0.25$ as suggested in [4] yields $B/A \approx 1.06$ and $A \approx 4$, meaning that at "four-times oversampling" in time-frequency, we can set $\widetilde{\phi}_{m,n} = \phi_{m,n}$ in (4) to a close approximation.

In the wavelet case, using a Klauder function with $\alpha = 250$ and $\beta = 100$ on the normalized frequency axis $0 < f < 1$, we obtain a snug frame at approximately eight times the redundancy of a wavelet orthonormal basis (see Table 1).

For computational purposes, it is convenient to choose the scale parameter $a_0 = 2$. However, to obtain a snug frame with the Klauder wavelet, we must in turn set $t_0 < 1$, which would lead to problematic non-integer time shifts nt_0 in our atoms. One way around this difficulty is the concept of *voices* [5]. The basic idea is to interlace in frequency several (not necessarily snug) frame decompositions to create one equivalent snug decomposition (see

Figure 2). In our case, the mother wavelet for each of our J voices is obtained from the Klauder function (10) by the rational scaling

$$H^{\nu}(f) \;=\; H(2^{\nu/J} f), \qquad \nu \;=\; 0, \ldots, J-1.$$

In Table 2, we give the frame bounds for several different J-voice wavelet frames constructed using $t_0 = 1$, $a_0 = 2$, and a Klauder function with parameters $\alpha = 250$ and $\beta = 100$. We chose $J = 5$ for our final implementation. From Table 1, we know that we can obtain a snug frame using $t_0 = 1$, $a_0 = 1.13$, and $J = 1$. Since $1.13^5 \approx 2$, it is no surprise that we can also achieve a snug frame using $t_0 = 1$, $a_0 = 2$, and $J = 5$.

3.4 Hybrid System

Using Klauder wavelet atoms as building blocks, we can decompose the Bertrand distribution into a sum of auto- and cross-Bertrand distributions. By limiting the interaction of the atoms according to their distance, we can both retain the (useful) local nonlinear interactions and suppress the (nuisance) global interactions. Denoting the distance metric by D_{L}, we have

$$\widehat{B}_s(t,f) \;=\; \sum_{(m,n)} |d_{m,n}|^2 \, B_{\psi_{m,n}}(t,f) \;+\; \sum_{0<D_{\mathrm{L}}[(m,n),(m',n')]\leq\delta} d_{m,n}\, d^*_{m',n'}\, B_{\psi_{m,n},\,\psi_{m',n'}}(t,f), \qquad (12)$$

with $\widehat{B}_s \;\to\; B_s$ as $\delta \;\to\; \infty$. The natural distance measure for time-scale analysis is the *Lobachevsky metric* [10]. With this measure, the distance between two wavelet atoms at location (m,n) and (m',n') is defined as

$$D_{\mathrm{L}}[(m,n),(m',n')] \;=\; \cosh^{-1}\left\{1 + \frac{nn'}{2f_c^2 a_0^{m+m'}} \left[t_0^2(na_0^m - n'a_0^{m'})^2 + (a_0^m - a_0^{m'})^2\right]\right\},$$

with f_c a reference frequency. In contrast to the time and frequency shift invariant Euclidean and Manhattan distances, the Lobachevsky distance is time-shift and scale-change invariant. Figure 3 shows iso-contours of this distance superimposed on a 3-voice wavelet frame pattern.

As a simple enhancement to the hybrid scheme, we can taper the influence of the interference components as the distance D_{L} increases. We do this by replacing the second term on the right side of (12) with

$$\sum_{(m,n)\neq(m',n')} T\{D_{\mathrm{L}}[(m,n),(m',n')]\}\, d_{m,n}\, d^*_{m',n'} B_{\psi_{m,n},\,\psi_{m',n'}}(t,f),$$

with $T(x)$ a smooth tapering function such that $T(0) = 1$ and $\lim_{x\to\infty} T(x) = 0$. The setup (12) is a special case of the above with T a step function. This enhancement applies equally well to the hybrid time-frequency scheme of (6).

4 Implementation

The time-scale distribution series (12) has been implemented and performs well. However, lack of a closed form expression for the Bertrand distribution of the Klauder function limits the computational efficiency of the technique. For applications in which computation and storage are at a premium, we have developed an approximation to (12) with the following justification:

1. Even when the signal we analyze is wide-band, each local cross-Bertrand distribution involved in (12) is reasonably narrow-band given the narrow bandwidth of the Klauder wavelets and the fact that they interact at small distances only. Thus, since the Bertrand and Wigner distributions resemble one another closely for narrow-band signals [7], it is reasonable to replace the Bertrand distribution in (12) with the Wigner distribution.

2. For large values of β, the Klauder wavelet can be approximated using a modulated Gaussian (Morlet) wavelet $r(t) = e^{-t^2/2\sigma^2}\, e^{i2\pi f_c t}$ with $\sigma = \alpha/(\pi\sqrt{2\beta+1})$ and $f_c = (2\beta+1)/(2\alpha)$.

With the change to a Wigner distribution and Morlet wavelet analysis, we obtain closed form expressions for the auto- and cross-Wigner distributions in the approximation to (12). The Wigner distribution of a Morlet wavelet is the 2-d Gaussian $W_r(t,f) = 2\sigma\sqrt{\pi}\,\exp(-t^2/\sigma^2)\,\exp(-(2\pi\sigma(f-f_c))^2)$. The cross-Wigner distribution between a Morlet wavelet $r(t)$ and a shifted and scaled version of itself $q(t) = a_0^{-1/2}\, r((t-t_0)/a_0)$ is given by

$$W_{r,q}(t,f) = \sqrt{\frac{\pi}{C_1}}\,\exp\left\{\frac{(C_2+jC_3)^2}{4C_1}\right\}\exp\left\{-\frac{t^2}{2\sigma^2}-\frac{(t-t_0)^2}{2\sigma^2 a_0^2}\right\}\exp\left\{j2\pi f_0\left(t-\frac{t-t_0}{a_0}\right)\right\},$$

with $C_1 = \frac{1}{8\sigma^2}(1+1/a_0^2)$, $C_2 = -\frac{1}{2\sigma^2}(t-(t-t_0)/a_0^2)$ and $C_3 = \pi(f_0+f_0/a_0-2f)$. The results obtained using (12) and its Wigner/Morlet approximation show only very slight differences.

Figures 4, 5, and 6 illustrate the performance of the new hybrid time-scale distribution. In Figure 4, we exhibit the concentration/interference trade-off of the scheme *vs.* the threshold distance δ in (12). In Figure 5, we analyze a multicomponent synthetic signal. In Figure 6, we analyze a "click" signal of a bottle-nose dolphin. Hybrid time-scale analysis combines the high resolution of the Bertrand and Wigner distributions with the quasi-linearity of the scalogram (squared magnitude of the wavelet transform).

5 Conclusions

In this paper, we have developed a new approach to time-scale analysis that offers an easily controlled tradeoff between linearity and bilinearity. Throughout our development, we have stressed the use of the right ingredients for time-scale analysis. The Bertrand distribution, wavelet frame with minimum uncertainty Klauder wavelet, and Lobachevsky time-scale distance combine to form a representation capable of matching a broad class of wide-band signals.

Acknowledgments: The authors thank William Williams of the University of Michigan for the bottle-nose dolphin click signal and for permission to use it in this paper.

References

[1] L. Cohen, *Time-Frequency Analysis*. Englewood Cliffs, NJ: Prentice-Hall, 1995.

[2] O. Rioul and P. Flandrin, "Time-scale energy distributions: A general class extending wavelet transforms," *IEEE Trans. Signal Processing*, vol. SP-40, pp. 1746–1757, July 1992.

[3] S. Qian and J. M. Morris, "Wigner distribution decomposition and cross-terms deleted representation," *Signal Processing*, vol. 27, pp. 125–144, May 1992.

[4] S. Qian and D. Chen, "Decomposition of the Wigner distribution and time-frequency distribution series," *IEEE Trans. Signal Processing*, vol. 42, pp. 2836–2842, Oct. 1994.

[5] I. Daubechies, *Ten Lectures on Wavelets*. SIAM, 1992.

[6] J. Bertrand and P. Bertrand, "A class of affine Wigner functions with extended covariance properties," *J. Math. Phys.*, vol. 33, pp. 2515–2527, July 1992.

[7] P. Flandrin and P. Gonçalvès, "Geometry of affine time-frequency distributions," *Applied and Computational Harmonic Analysis*, vol. 3, pp. 10–39, Jan. 1996.

[8] J. R. Klauder, "Path integrals for affine variables," in *Functional Integration Theory and Applications* (J. P. Antoine and E. Tirapagui, eds.), p. 101, Plenum, New York, 1980.

[9] P. Flandrin, "On separability, positivity and minimum uncertainty in time-frequency energy distributions," 1996. in preparation.

[10] I. Daubechies, J. R. Klauder, and T. Paul, "Wiener measures for path integrals with affine kinematic variables," *J. Math. Phys.*, vol. 28, pp. 85–102, Jan. 1987.

Table 1: *Frame bounds for wavelet frames generated using a Klauder wavelet ($\alpha = 250$ and $\beta = 100$). We fix the time-step parameter at $t_0 = 1$ and vary the scale parameter a_0.*

a_0	A	B	B/A
1.44	0.43	6.28	14.3
1.27	2.82	6.31	2.24
1.15	7.86	8.07	1.027
1.14	8.44	8.56	1.013
1.13	9.09	9.14	1.006

Table 2: *Frame bounds for J-voice wavelet frames generated using a Klauder wavelet ($\alpha = 250$ and $\beta = 100$). We fix $t_0 = 1$, $a_0 = 2$, and vary the number of voices J.*

J	A	B	B/A
2	1.4	14.2	10.0
3	7.5	14.3	1.90
4	13.4	15.6	1.16
5	17.9	18.4	1.02
10	36.3	36.3	1.00

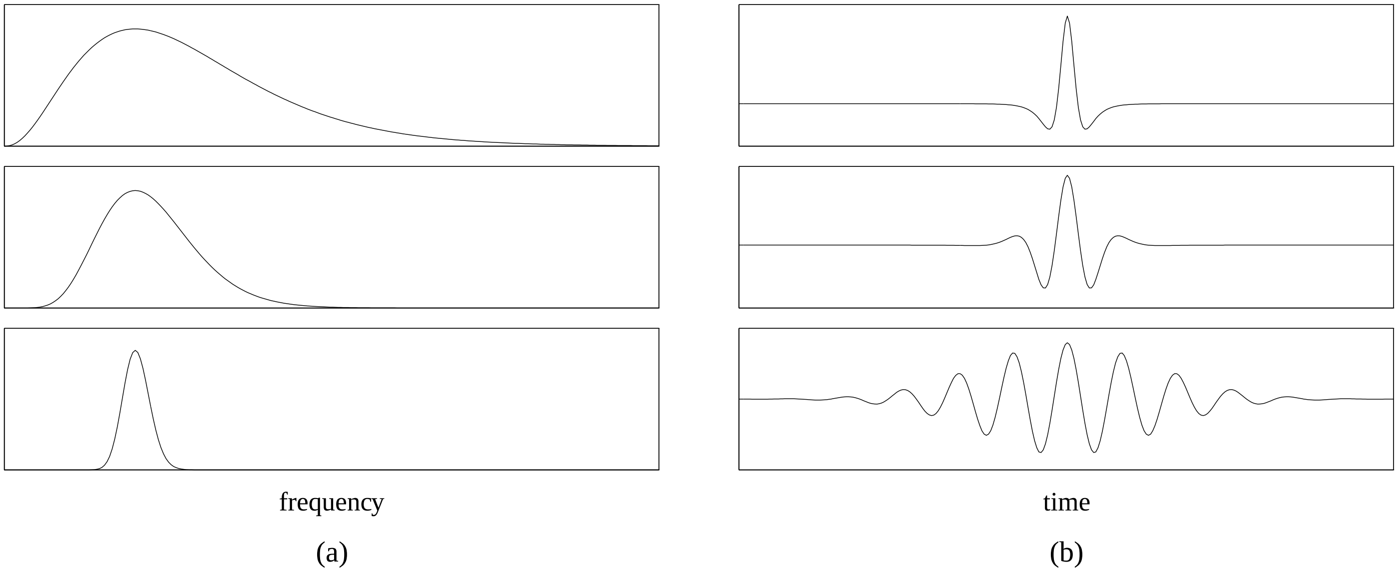

Figure 1: *(a) Spectrum* $|H(f)|^2$ *and (b) time waveform* $h(t)$ *of the Klauder wavelet (10) for different values of the parameters* α *and* β*. From top to bottom:* $\alpha = 12,\ \beta = 2.4\ (f_0 = 0.2\ Hz,\ Q = 1)$ *;* $\alpha = 42,\ \beta = 8.5\ (f_0 = 0.2\ Hz,\ Q = 2)$ *;* $\alpha = 500,\ \beta = 100\ (f_0 = 0.2\ Hz,\ Q = 7)$.

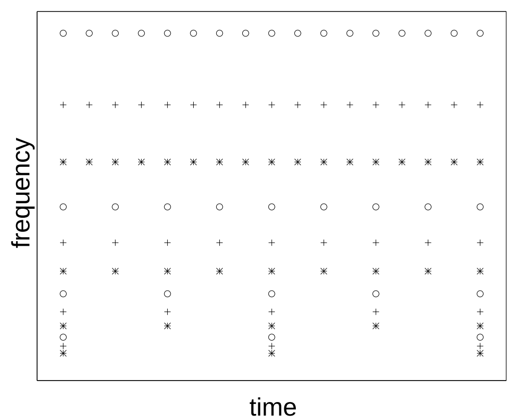

Figure 2: *Time-frequency tiling corresponding to a 3-voice wavelet-frame. Each of the symbols* $\circ$, $+$ *and* $*$ *represents a dyadic frame based on one of the 3 mother wavelets* $H^\nu(f) = H(2^{\nu/J} f),\ \nu = 0, 1, 2$.

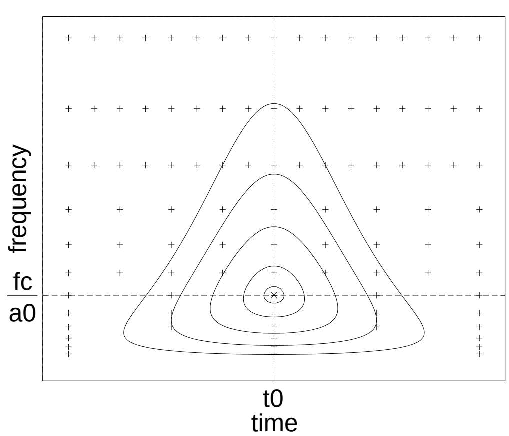

Figure 3: *Iso-contours of the Lobachevsky distance between the reference point* (t_0, a_0) *and the other locations of a 3-voices wavelet frame pattern.*

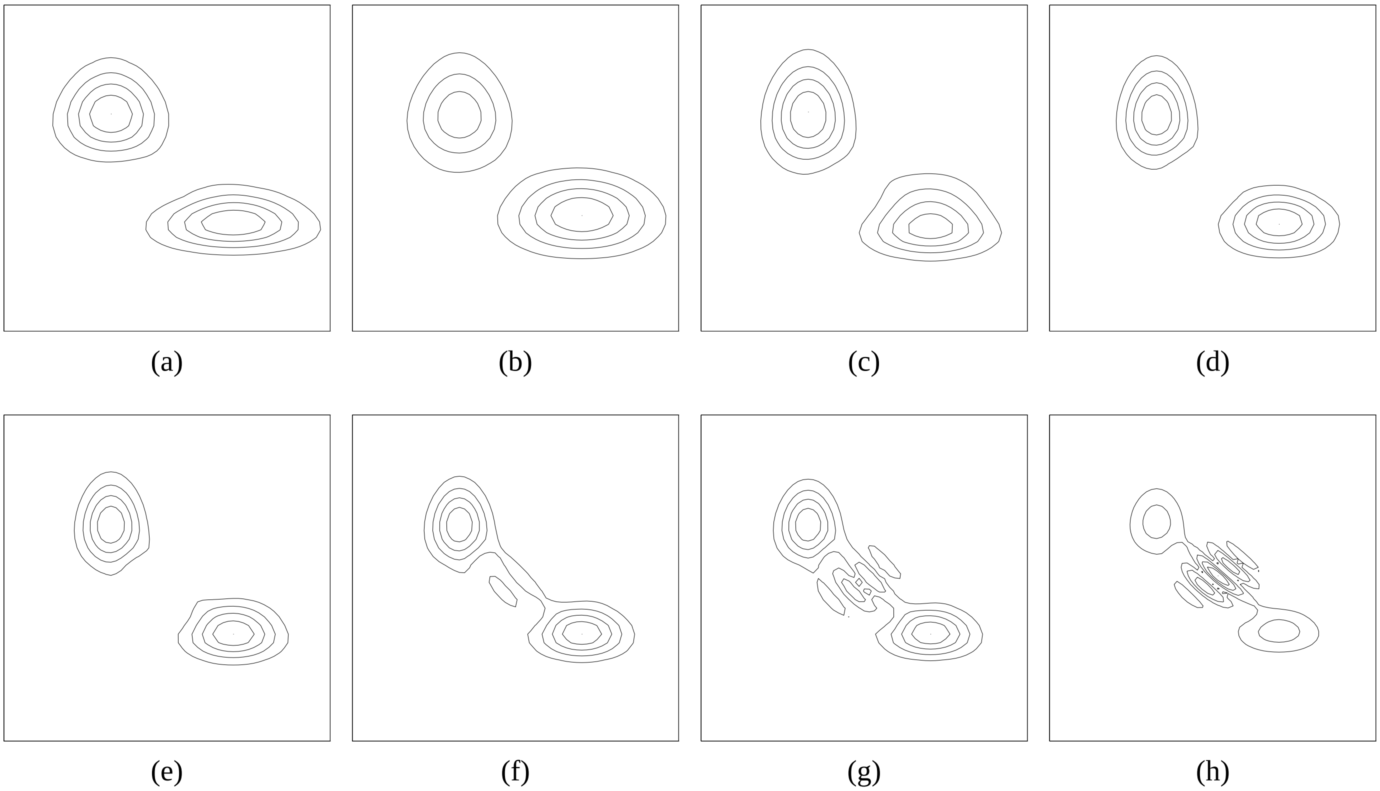

Figure 4: *Concentration vs. interference trade-off of the hybrid linear/nonlinear time-scale analysis scheme (12) as a function of the distance threshold* δ*. We compare (a) the scalogram (squared magnitude of the continuous wavelet transform) with hybrid representations of (b)* $\delta = 0$*, (c)* $\delta = 0.1$*, (d)* $\delta = 0.2$*, (e)* $\delta = 0.3$*, (f)* $\delta = 0.4$*, (g)* $\delta = 0.6$*, and (h)* $\delta = \infty$ *(Wigner distribution). We employ the Wigner/Morlet approximation of Section 4. Horizontal axis corresponds to time, vertical axis to frequency.*

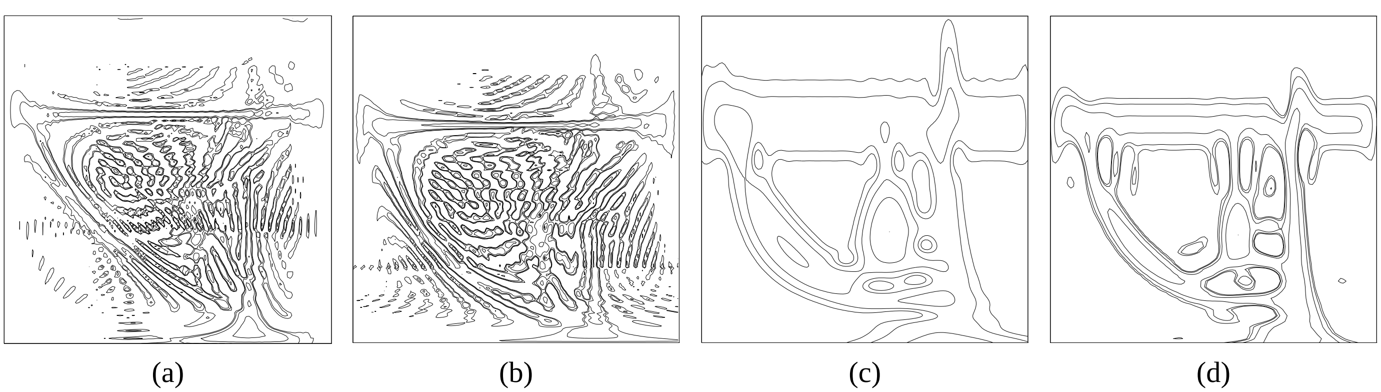

Figure 5: *Time-frequency and time-scale distributions of a test signal composed of a sinusoid, a hyperbolic chirp, a Klauder wavelet pulse, and a local singularity of the form* $|t - t_0|^{-0.15}$*. Horizontal axis corresponds to time, vertical axis to frequency. (a) Wigner distribution. (b) Bertrand distribution. (c) Scalogram. (d) Hybrid linear/nonlinear time-scale representation (12) with interaction distance* $\delta = 0.5$*.*

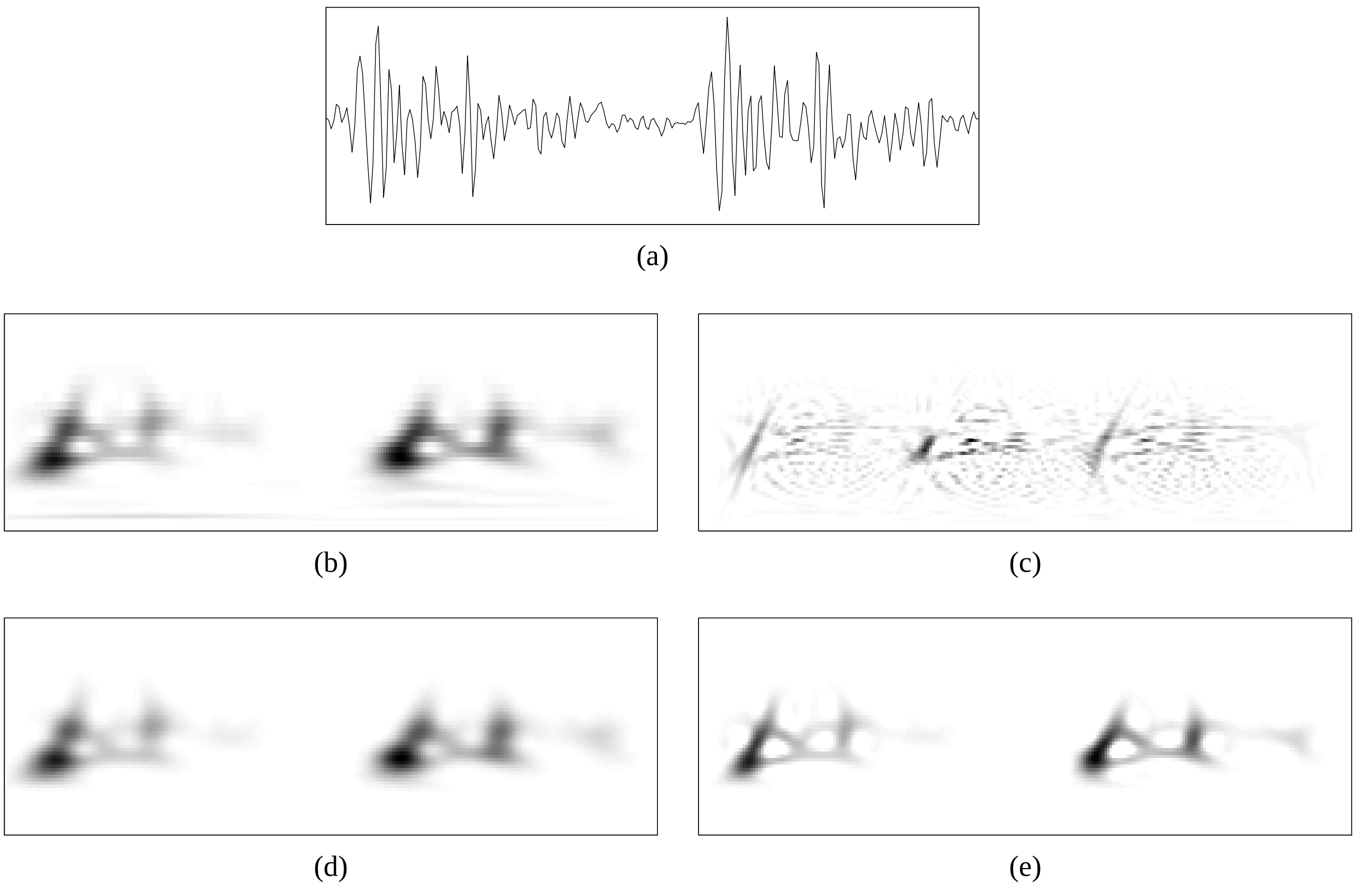

Figure 6: *Time-scale distributions of two "clicks" emitted by a bottle-nose dolphin. (a) Time signal. (b) Scalogram. (c) Wigner distribution. (d) Hybrid time-scale distribution, $\delta = 0.2$. (e) Hybrid time-scale distribution, $\delta = 0.5$.*